Aerosol Backscatter Coefficient Profiles Measured at 10.6 μm

R. L. SCHWIESOW, R. E. CUPP, V. E. DERR, E. W. BARRETT AND R. F. PUESCHEL

NOAA Environmental Research Laboratories, Boulder, CO 80303

P. C. SINCLAIR

Atmospheric Science Department, Colorado State University, Ft. Collins 80521

(Manuscript received 1 April 1980, in final form 30 November 1980)

ABSTRACT

Using an airborne lidar, we have measured atmospheric aerosol backscatter coefficients (differential backscatter cross section per unit volume) for 10.6 μm wavelength laser radiation as a function of height to 5200 m for a number of meteorological conditions over the United States high plains. Airborne *in situ* samplers measured the particle size distribution at the same time and altitude as the lidar measured backscatter. One backscatter coefficient profile at 10.6 μm was compared with a 0.694 μm lidar backscatter profile as well as with the particle size distribution profile. The average infrared backscatter coefficient ranged from $\sim 8 \times 10^{-9}$ m^{-1} sr^{-1} at the surface to 1×10^{-10} m^{-1} sr^{-1} at 5200 m altitude.

1. Purpose

This study attempts to determine the height profile of atmospheric aerosol backscatter coefficient for 10.6 μm wavelength radiation. Since backscatter profiles depend on location, season, current weather conditions, air mass history, and other variables, one experiment can cover only a limited range of conditions. Our objective was to measure representative values of the backscatter coefficient in relatively clean air that was free of fog, cloud and urban concentrations of anthropogenic aerosol. A study of the backscatter profile includes characterizing the atmospheric conditions in a useful way, such as aerosol size distribution profiles.

A direct application of 10.6 μm backscatter profiles is to estimate the performance of CO_2 laser lidar systems that make wind measurements in the cloud-free atmosphere. Another use is for input to atmospheric models that study radiation balance and its relationship to climate change.

We are not aware of any other measurements of 10.6 μm wavelength backscatter profiles in the atmosphere. Previous visible wavelength (usually ruby laser) backscatter measurements are discussed later. Aerosol size distribution profiles have also been measured and/or postulated for typical atmospheres, but the connection between aerosol concentration and infrared backscatter involves an assumption of refractive index (and its distribution within the particle). Our goal was to measure infrared backscatter values directly and provide a set of calibrated infrared backscatter coefficients *in absolute units*.

2. Experiment

a. Approach

We used a CO_2 laser transmitter in a calibrated lidar aboard a light aircraft to obtain data from greater heights and with better height resolution than could be achieved with a similar ground-based lidar. To partly characterize the aerosol environment as close in space and time as possible to the lidar backscatter measurements, we flew *in situ* aerosol samplers in another aircraft.

Because atmospheric backscatter coefficients vary widely in time and space, we chose to average the measured profiles to produce representative profiles of backscatter coefficient and aerosol particle concentration. Minimum and maximum observed backscatter values give an indication of the variability in the data. One case study is included to show typical variations of backscatter with altitude, to compare 10.6 μm backscatter with the only 0.694 μm backscatter data available during the experiment, and to allow a direct comparison of backscatter and aerosol data. A detailed study of the backscatter coefficient profile at visible wavelengths was not an objective of our experiment. Because visible-wavelength data are only auxiliary information, visible lidar techniques and uncertainties are treated in much less detail than the infrared lidar approach.

b. Conditions

Backscatter and aerosol profiles were measured in the region of Boulder, Ft. Collins and Greeley,

0021-8952/81/020184-11$06.75

TABLE 1. Experiment conditions.

Date (1978)	Time (MST)	Number and location of profiles	Estimated visibility (km)		Surface temperature (°C)	Clouds
			Surface	Aloft		
27 Feb	1600–1715	1 Greeley	>50	>50	0	altostratus overcast, light snow on ground
28 Feb	1430–1545	1 Greeley	—	>100	2	scattered altocumulus, broken west, clear east
4 Mar	1330–1500	1 Greeley	30	>50	1	thin cirrus, brown haze on surface, scattered cumulus west
7 Mar	1200–1500	2 Boulder	>50	>100	5	clear, cumulus humilis west, precipitation preceding 18 h
8 Mar	1015–1200	1 Boulder	>100	>180	5	thin cirrus, 80% coverage
visible lidar comparison						
9 Mar	1500–1645	1 Boulder	—	—	10	broken altocumulus overhead and west, cirrus east, cloud base ~ 2.8 km
16 Mar	1045–1300	2 NE of Ft. Collins	50	90	0	scattered cirrus, few altocumulus based at 3.9 km, surface haze
high altitude						
21 Mar	1145–1445	2 Boulder, Ft. Collins	50	>80	15	scattered cirrus, surface haze, strong wind preceding 24 h

Colorado, over semi-arid high plains. Ground level in the experimental area is ~1.6 km above sea level. Eleven profile runs produced useful data. A profile was determined on each ascent or descent for which complete backscatter and aerosol data were obtained; ascents and descents for a single flight often sampled different locations.

All measurements were made in cloud-free regions of the atmosphere during the period 27 February–21 March 1978. Table 1 lists the days in which measurements were made and gives notes on weather conditions. Visual ranges were estimated by an observer noting what features (mountains, grain elevators, towns, etc.) were clearly visible and measuring the distance to the feature on an aeronautical sectional chart.

Weather conditions for the case study data on 8 March 1978 were dominated by a surface high ~ 250 km west of the measurement area. A frontal passage 36 h before the measurement time produced light precipitation over a wide area and probably significant precipitation scavenging of the aerosol population. Surface winds were light and variable, and winds aloft were from the north. The 500 mb height contours implied subsidence at that level.

c. *Measurement technique*

The amount of 10.6 μm laser radiation backscattered by the atmosphere was measured with a calibrated continuous wave (cw) Doppler lidar (Schwiesow and Cupp, 1980). The lidar, carried in a light aircraft, was focused at a range of 500 m to the side of the aircraft. Backscatter data were smoothed by a 5 s time constant filter before recording, which resulted in spatial averaging over a volume approximately 500 m × 300 m in horizontal dimensions and 6 m in the vertical. The prerecording time constant was chosen to be long enough to improve the signal to noise over the raw spectral data and short enough to be less than the period of changes in air speed, which cause changes in spectral position. The scattered flux value was further time-averaged after recording, depending on the climb or descent rate of the aircraft, to give an average backscatter value for each 50 m height increment.

The backscattered flux measurements are reduced to, and reported as, a backscatter coefficient, which is the ratio of backscattered to incident radiant power per length of the scattering region and per solid angle of the receiver aperture as seen from the scattering region. The length of the scattering region is taken as the distance between the 40% power response points for the lidar, based on the variation of radiant flux density along the axis of a Gaussian beam truncated at the aperture (Dickson, 1970). The effective length of the scattering region then is 12 m ± 10% if focused at a range of 100 m, and varies as the square of the

focal distance. For a focused cw lidar, the product of the length of the scattering region and the solid angle of collection is independent of range.

One unusual characteristic of a homodyne Doppler lidar is that it operates with extremely high spectral resolution. In this case the instrumental resolution is 100 kHz. Because of the Maxwell-Boltzmann velocity distribution of the molecules, the Rayleigh (molecular) scattering linewidth is approximately equivalent to a rectangular function 1.4×10^5 kHz wide for the scattering of 10.6 μm radiation. The aerosol scattering linewidth is somewhat narrower than 100 kHz. Therefore, the aerosol signal appears on top of a spectrally wide and flat baseline of Rayleigh scattering, which cannot be distinguished from the shot noise on the local oscillator signal. The particle scattering is determined from the signal above the baseline.

As a consequence, the Doppler lidar measures particle scattering only. Using high spectral resolution to separate molecular and particle backscatter contributions has been used in the visible spectral region by Fiocco *et al.* (1971). If integrated over the actual Rayleigh linewidth of $\sim 5 \times 10^5$ kHz, the Rayleigh backscattering coefficient for a midlatitude standard atmosphere is 7.8×10^{-12} m^{-1} sr^{-1} at 1.6 km ASL (0 km AGL). This molecular backscatter coefficient is larger than the system threshold sensitivity for 100 kHz signals (discussed later), but it is orders of magnitude too small to be detected by the lidar if the bandwidth of the system were increased to accept signal and noise over a 5×10^5 kHz spectral interval, which would include all of the Rayleigh scattering.

A ground-based, vertically pointing, pulsed ruby lidar was used to give profiles of visible (0.694 μm) backscatter. It was calibrated with a target of known diffuse reflectance. Complete space-time overlap between ruby lidar and aircraft-based data was not possible because of aircraft climbing time. Data were taken when the 10.6 μm lidar was nearly over the ground-based system and was at 2.2 km altitude.

In contrast to the infrared Doppler lidar, which measures only particle backscattering, the spectral bandpass of the pulsed ruby lidar is larger than the Rayleigh scattering linewidth. Therefore the visible wavelength lidar measures the backscatter coefficient from particles and molecules. The molecular backscatter coefficient for a midlatitude standard atmosphere is 4.3×10^{-7} m^{-1} sr^{-1} at 1.6 km ASL, for example, which is a significant part of the total measured backscatter coefficient. Because the ruby lidar measures the sum of particulate plus molecular scattering, we do not separate the components in reported data.

Two airborne particle size spectrometers covering different size ranges measured the aerosol concentration profiles. The lidar and aerosol measuring aircraft were separated by ~1 km at the same altitude and flown in a pattern that ensured that neither aircraft would contaminate the measurements of the other. The operation of the spectrometers relies on near-forward-angle light scattering. To reduce the large statistical fluctuations, which result when there are few particles in each size interval, data were averaged for 120 s, or ~36 m in altitude. Particle concentrations were smoothed with a sliding average over three adjacent particle size intervals (e.g., $r = 3.0$ to 3.5 μm) and further averaged over times appropriate for a 100 m height increment. Size distribution spectra in the form $dn/d(\ln r)$ vs r, where n is the number density of all particles with radii $< r$, were read at radii of 0.1, 0.5, 1.5, and 3.0 μm to give the number density of particles per unit interval of r at radius r.

d. Measurement accuracy

The uncertainty in the atmospheric backscatter coefficient is dominated by uncertainty in the calibration measurement of the lidar return from the standard target performed before and after each flight. This reading uncertainty is ±2 dB (a factor of ~1.6 or ±60%) on the absolute backscatter. Uncertainties are measured in dB because the output of the spectrum analyzer is logarithmic, given as dB with respect to a reference power level (Schwiesow and Cupp, 1980). The ±2 dB uncertainty applies to all backscatter coefficient determinations because all measurements are referred to the return from the standard target. Relative backscatter during a single profile is uncertain between the limits ±0.3 to ±0.6 dB depending on whether the backscatter is greater or less than 10 dB above the threshold of detection. These values were based on observations of fluctuations of the signal level. Other contributors to uncertainty in the backscatter coefficient are the length of the scattering volume (±10%) and the diffuse reflectance of the reference scattering target (±12%). The overall uncertainty in reported backscatter coefficient is the larger of ±2.5 dB or the detection threshold. Uncertainties (dB) are added to obtain an overall uncertainty in the same way that fractional uncertainties of factors are added to estimate the uncertainty of a product. We chose to add uncertainties linearly rather than as the root of the sum of squares so that the uncertainty estimate would be conservative.

The coherently detected signal power from the standard target fluctuated in time. If the statistical distribution of the magnitude of these fluctuations was not symmetric about the mean, it is possible that a systematic error of up to 2 dB existed in the estimate of the average values of the return from the standard target (Schwiesow and Cupp, 1980). Signal statistics were not measured in this

experiment but were assumed to be approximately symmetrically distributed about the mean on the basis of qualitative observations.

The detection threshold of the system (signal-to-noise approximately equal 1) corresponds to a backscatter coefficient of 2.4×10^{-12} m^{-1} sr^{-1} ± 2.5 dB for a cw signal, representative of an ideally homogeneous atmosphere, time-averaged by a 5 s time constant filter. Actual scattering data in weak scattering conditions were intermittent on time scales shorter than the 5 s integration time of the system, so that it was impossible to determine backscatter coefficients to the precision implied by the cw detection threshold. From the artificial quantization in the weak signal data, the detection threshold and resolution for intermittent scattering corresponds to a 5 s average backscatter coefficient of $\sim 3 \times 10^{-12}$ m^{-1} sr^{-1}. Fluctuating data falling within 3×10^{-12} m^{-1} sr^{-1} of convenient fiducial points were assigned to the center of the range to avoid implying more resolution than actually exists.

The overall uncertainty in measured backscatter at 0.694 μm is approximately ±2 dB. The uncertainty is caused by changes in transmitter and receiver beam overlap as the lidar is scanned from horizontal elevation for calibration to vertical and by uncertainties in the standard target diffuse reflectance and return signal level. The uncertainty value is checked by comparing measured and calculated Rayleigh return from presumed aerosol-free altitudes.

The absolute accuracy of aerosol particle concentration measurements is an active area of research (Lundgren *et al.*, 1979), and the evaluation of an overall uncertainty is beyond the scope of this study. The uncertainty in reading the particle size spectrometer is the greater of $\pm 5 \times 10^2$ m^{-3} or ±15%, and is caused by departures of the measured size spectra from a smooth curve. Because of height averaging over 100 m, sliding-average spectral smoothing, and overlapping spectrometer ranges, each aerosol concentration measurement represents ~12 min of data. Average profiles represent an increase in data-taking time per point. This is necessary for large particles and high altitudes where statistical uncertainty on the total number of particles counted becomes important.

3. Results

a. Atmospheric backscatter coefficient

Fig. 1 shows observed values of the atmospheric backscatter coefficient at 10.6 μm wavelength as a function of height above the surface. The measured backscatter coefficient includes the effects of aerosol particle concentration, size distribution and refractive index.

The three data points plotted at each 50 m height increment (to 4 km) represent the minimum, average and maximum backscatter coefficients observed during the 11 profile runs for which valid backscatter data and aerosol concentration data were obtained. Above 4 km only an average is shown, and only one profile (not an average) extends above 4.5 km. The number of measured profiles contributing to the data set at each height is indicated by the histogram.

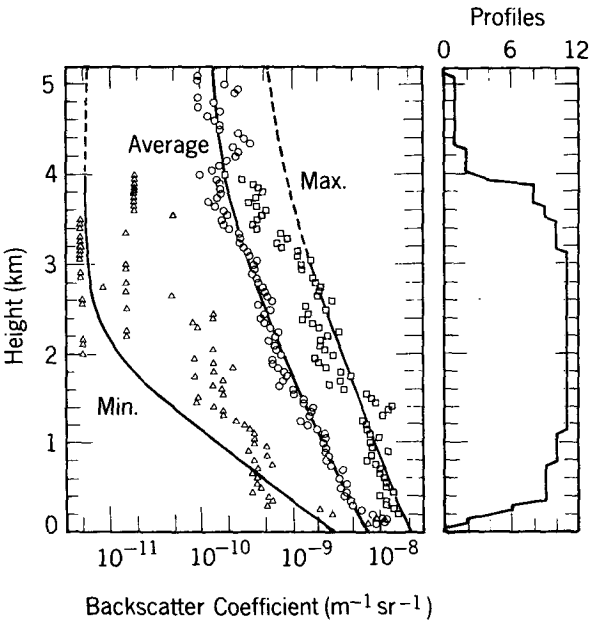

FIG. 1. Backscatter coefficient measured at 10.6 μm wavelength above east-central Colorado. Data for these profiles are taken from all individual profiles. At each 50 m increment from 100 m to 4 km above the surface, the average, minimum and maximum observed backscatter coefficients are plotted on a logarithmic scale. The graph on the right margin gives the number of data runs considered at each height on a scale of 0 to 11.

Backscatter coefficients vary widely in time and space. Even for the small range of atmospheric conditions involved in this study, minimum and maximum values are separated by a factor of 10 near the surface and of 100 near 2.5 km height. Because of the layered structure of individual profiles, no particular run consistently gave minimum or maximum values of backscatter for contiguous height intervals. The residual departures of the average data from a smooth curve (the order of 10%) show the effect of spatial inhomogeneities even when they are filtered by the averaging process.

Based on the data, we suggest an analytic model for backscatter of 10.6 μm radiation in the lower atmosphere of the form

$$\beta_{\pi,10.6}(z) = \beta_0 \exp(-mz) + \beta_c, \quad z \leq Z, \quad (1)$$

where $\beta_0 + \beta_c$ is the backscatter coefficient at the surface and β_c is a limiting value at the mid-tropo-

TABLE 2. Model backscatter profile coefficients.

Model	β_0 (m^{-1} sr^{-1})	m (km^{-1})	β_c (m^{-1} sr^{-1})
Average	744×10^{-11}	1.15	14×10^{-11}
Minimum	303×10^{-11}	3.0	0.55×10^{-11}
Maximum	2298×10^{-11}	0.92	43×10^{-11}

spheric height at which our experiment stopped (Z = 5.2 km). Variable z is height above ground (AGL). We call Eq. (1) with coefficients that represent the backscatter at each height averaged over all measured values the average model profile. The equation with other values for the coefficients can be made to fall to the weak-signal side of most of the data points that are the minimum backscatter observed from all measurements. We term this the minimum backscatter model profile. Eq. (1), with coefficients to place the curve to the strong-signal side of the data points that are the maximum observed at any height from all the profiles, represents a maximum backscatter model profile. The maximum and minimum values at any height are more subject to statistical variation than the average value. Therefore, a few extreme data points are allowed to fall outside the minimum and maximum model profiles so that the general shape of the curves and the values for the majority of the data are well-represented. Coefficients for the three models are given in Table 2, and model curves are drawn in Fig. 1. These models are not least-squares fits to the data, but are intended to present the general characteristics of the observations in a simple form.

A more conceptually satisfying model than (1) would be a two slope model of form

$$\beta_{\pi,10.6}(z) = \beta_0 \exp(-mz) + \beta_c \exp(-qz), \quad z \leq Z. \quad (2)$$

However, our data do not extend to large enough z to evaluate q except to say that $q \ll m$. We therefore set $q = 0$ rather than speculated on its value.

The average backscatter data fall close to the model representation at all heights, with increasing fluctuations as the number of data samples becomes small. Above 3 km the maximum data begin to fall below the model as fewer and fewer runs are considered. There are no experimental data on which to base β_c for the maximum curve, so the ratio of maximum to average β_0 was used to set the maximum β_c from the average value for β_c. The evidence to suggest a lower-limit constant β_c is particularly strong in the minimum signal case. A simple exponential decrease (linear on the semi-log plot) does not represent the profiles of averaged backscatter and minimum observed backscatter.

The exponential model (1) has limitations. An individual backscatter profile is often strongly stratified and does not generally follow an exponential form. However, when all 11 profiles are considered, the *average* is characteristic of a well-mixed atmosphere with an exponential profile. The backscatter is not likely to be as large as β_c to the top of the atmosphere. Therefore, we must either terminate the model at Z = 5.2 km, introduce a nonzero q in (2), or choose a different model for high altitudes.

The results of our measurements show that the backscatter coefficient falls off more slowly with height when the scattering is strong. In weak signal situations, where the backscatter decreases more rapidly with height than for strong signal, the coefficient approaches a nearly constant value at lower heights above the surface than it does in the case of large signal. Fig. 1 illustrates these relationships. If the scattering is less than average near the surface, it will be an even smaller fraction of the average aloft.

b. *Supporting data*

Aerosol concentration profiles are one characteristic of the state of the atmosphere. Fig. 2 presents the average aerosol concentration profiles observed during the experiment. At each height the averaged data points (in order of increasing concentration) are for particle size ranges centered at radii of 3.0, 1.5 and 0.5 μm with a window ~ 15% of the center value.

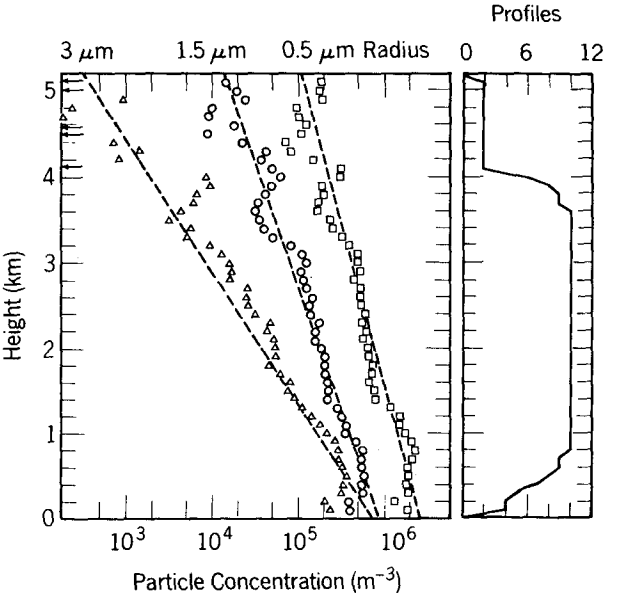

FIG. 2. Average particle concentration in the form $dn/d(\ln r)$ as a function of height above the surface. In the order of increasing concentration, the interval-normalized logarithmic profiles are for particles of radii 3, 1.5 and 0.5 μm. Dashed lines give model profiles. Arrows on the left margin indicate data off scale toward lower concentrations.

Spatial inhomogeneities persisting in the averaged data show larger variability in particle concentration than in backscatter coefficient. This comparative variability results partly because the sample volume is much larger for backscatter than for aerosol concentration measurements. Averaging over multiple profiles reduces the effect of sample volume differences because profile-to-profile differences are generally larger than spatial inhomogeneities within a single profile. Another reason for the smaller variability of backscatter is that backscatter adds the effects from all aerosol sizes, whereas profiles for separate aerosol size ranges are plotted in Fig. 2. Values of minimum and maximum concentration for the three size ranges were not plotted because these values fluctuate widely and because they provide little if any information relevant to understanding the relationship between various backscatter profiles. To within the accuracy permitted by concentration inhomogeneities, the profile slopes for minimum and maximum concentration for each radius interval were identical to the slope of the corresponding average concentration profile.

There is no evidence in the aerosol size distribution data for a transition from an exponentially decreasing profile to a profile constant with height, as is observed from the backscatter data. Average concentrations exhibit different slopes for different particle radii when fitted with a straight exponential decrease. Fig. 2 shows dashed lines for fitting to a model of the form

$$dn(z)/d(\ln r) = c_0 \exp(-pz), \qquad (3)$$

where c_0 is a surface concentration. Table 3 gives the coefficients for models of the concentrations of the three particle radii graphed and for 0.1 μm radius particles. We have chosen p to represent the slope of the data over the range 0.5–5 km, ignoring the first 400 m of data because the lowest data are not consistent with a simple exponential model.

Individual aerosol concentration profiles are generally stratified and do not follow an exponential decrease. When all data for a particular size range at a given altitude are averaged, the resulting *average* aerosol concentration profiles do follow exponential forms. Averaged aerosol concentration profiles are similar to those of a well-mixed atmosphere with an exponential decrease of concentration with height.

The observed particle size distribution spectrum at a given height is generally bimodal. Peaks appear near 0.1 μm radius and 1.5–2 μm radius, with the latter peak being significantly broader on a logarithmic particle radius scale. The 1.5 μm peak, which is barely noticeable near the surface, increases with height, whereas the 0.1 μm peak decreases with height until it disappears at 5 km above the surface.

TABLE 3. Model aerosol profile coefficients.

Radius (μm)	c_0 (m^{-3})	p (km^{-1})
0.1	1.25×10^9	1.15
0.5	2.6×10^6	0.60
1.5	8.9×10^5	0.79
3.0	7.5×10^5	1.48

TABLE 4. Aerosol size distribution spectrum.

Height (km)	$\alpha(z)$	Log (excess concentration) 0.1 μm radius	Log (excess concentration) 1.5 μm radius
0.5	0.95	1.9	0
1	1.2	1.6	0.03
2	1.7	1.0	0.19
4	2.6	0	0.49

Fig. 2 and Table 3 show that a Junge power-law representation of the particle size distribution at any height z (AGL) in the form

$$dn/d(\ln r) = A(z)(r/r_0)^{-\alpha(z)}, \qquad (4)$$

where A is a scaling concentration, r_0 a scaling radius, and $\alpha(z)$ the power law coefficient at height z, is not representative of our observations. However, the data can be represented by a power law with excess concentration over the power law at 0.1 and 1.5 μm radius. Table 4 gives the observed power law coefficient at four different heights and the logarithm of the factor multiplying the base concentration at the two peaks. Because the concentrations are taken from the exponential model profiles of Fig. 2, the values in Table 4 are model values that are within approximately 25% uncertainty of the fluctuating actual measurements.

Average temperature and dewpoint soundings (taken at Denver) are shown in Fig. 3. Morning (1200 GMT) and evening (0000 GMT) profiles bracket the data flight times. Twelve profiles, two for each of six days, are averaged. Data for 27 February and 4 March 1978 are missing.

Six of the individual soundings showed strong drying beginning at heights between 2.0 and 4.0 km and averaging 3.1 km. However, the average profiles show only slight drying beginning at ~3 km. The Denver soundings were made between 45 and 110 km away from the flight locations and are only generally representative of conditions during profile measurement.

c. *Infrared and visible backscatter comparison case study*

The backscatter profile at 10.6 μm wavelength on the morning of 8 March 1978 is shown as the center trace on Fig. 4. The scattering in this case is slightly weaker than the average in Fig. 1. For

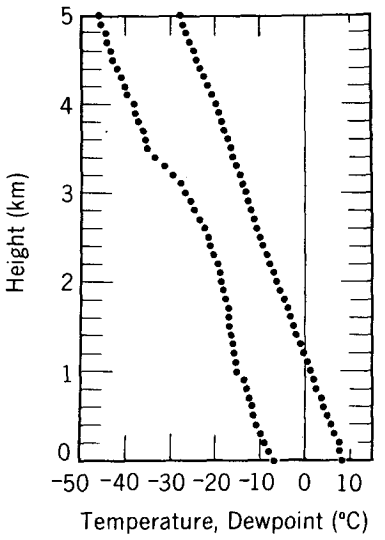

FIG. 3. Temperature and dewpoint profiles taken at Denver, averaged over the experiment. Morning (1200 GMT) and evening (0000 GMT) soundings are included for each of six days (data for 27 February and 4 March 1978 missing).

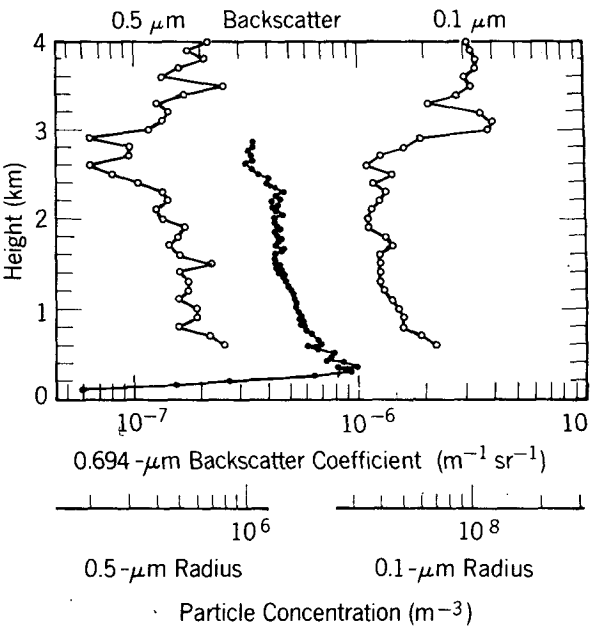

FIG. 5. Particle concentration and 0.69 μm backscatter coefficient profiles on a logarithmic scale for 8 March 1978. Data points are for the interval-normalized concentration of particles of 0.5 μm radius, backscatter coefficient, and interval-normalized concentration of particles of 0.1 μm radius, from left to right. The apparent decrease in backscatter below 0.3 km comes from incomplete overlap of transmitted and received lidar beams.

comparison, the center trace in Fig. 5 shows the 0.694 μm backscatter profile taken at approximately the same time and place with a ground-based lidar. The apparent decrease in backscatter below 0.3 km comes from incomplete overlap of transmitted and received lidar beams. The intervals on both logarithmic scales are the same. If we smooth the infrared backscatter profile to average over spatial inhomogeneities, we obtain the backscatter coefficients in Table 5.

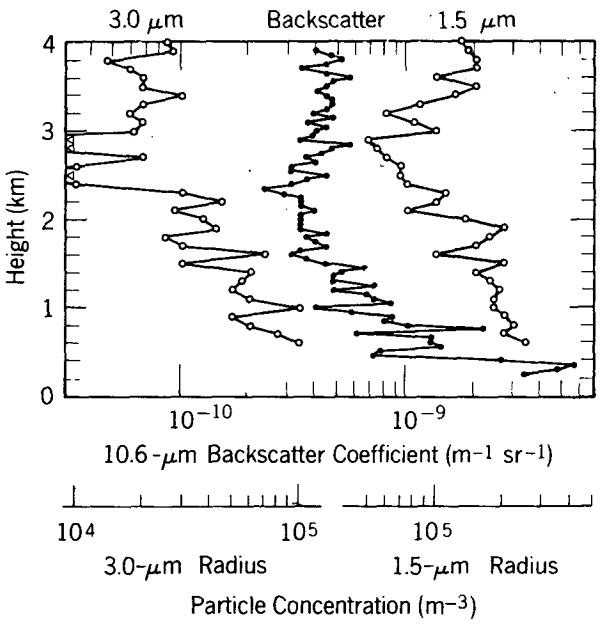

FIG. 4. Particle concentration and 10.6 μm backscatter coefficient profiles on a logarithmic scale for 8 March 1978. Data points are for the interval-normalized concentration of particles of 3.0 μm radius, backscatter coefficient, and interval-normalized concentration of particles of 1.5 μm radius, from left to right. Arrows on the left margin indicate data off scale toward lower concentrations.

Atmospheric aerosol profiles for 8 March 1978 are given in Figs. 4 and 5 and in Table 6. The slopes of the aerosol size distribution spectra (decrease of concentration with increasing particle size) change less with height than do average values and are smaller than average at 2 and 4 km. This greater-than-average ratio of large to small particle concentration favors a less-than-average decrease in infrared backscatter with height. Comparison of Figs. 1 and 4 shows that the ratio of backscatter from the 8 March case to the average is smaller near the surface than aloft. The region near 2.6 km altitude shows a relative minimum in aerosol concentration for the three larger particle ranges but is

TABLE 5. Infrared and visible backscatter coefficients (m^{-1} sr^{-1}).

Height (km)	Infrared	Visible	Ratio
0.6	1.8×10^{-9}	7.6×10^{-7}	4.2×10^{2}
1	7.6×10^{-10}	5.4×10^{-7}	7.1×10^{2}
2	3.9×10^{-10}	4.4×10^{-7}	11.4×10^{2}
2.8	4.5×10^{-10}	3.5×10^{-7}	7.7×10^{2}

not significant in the 0.1 μm radius particle profile. All size ranges show an increase in concentration beginning at 2.9 km height.

The average of morning and evening temperature and dewpoint soundings, taken approximately 4 h before and 6 h after the flight and 45 km distant, is shown in Fig. 6. The 10.6 μm backscatter shows the effect of the ground-based inversion, and the decrease in large-particle concentration corresponds roughly to the drying in the 2–3 km height range. Both moisture and large-particle concentration increase above approximately 3 km. Detailed comparisons between the backscatter and aerosol profiles and the temperature soundings are not appropriate because of the separation in space and time between the two measurements.

The infrared backscatter profile does not decrease as much as the 1.5 μm radius particle concentration in the relatively clean, dry layer near 2.6 km altitude, but in other height regions the backscatter profile appears to follow the height-smoothed, 1.5 μm particle concentration. The difference between the 10.6 μm and the 1.5 μm backscatter particle concentration profiles near 2.6 km may result from a reduction in the imaginary part of the effective aerosol refractive index in the dryer region. IR backscatter depends on aerosol concentration, the aerosol size distribution spectrum, and the aerosol refractive index, none of which can be considered uniform in space during even a single profile measurement.

The visible backscatter profile in Fig. 5 tends to follow the 0.5 μm profile, with some influence from the 0.1 μm profile, once full overlap between transmitter and receiver beams is achieved at ~400 m. Below 1.5 km all profiles in Fig. 5 are similar. Above that level, the visible backscatter neither drops with height as much as the 0.5 μm profile nor increases as much as the 0.1 μm profile. This is not surprising because the aerosol size parameter, $\sigma = 2\pi r/\lambda$ (where r is particle radius and λ the wavelength) is 1 for particles slightly larger than 0.1 μm. The scattering cross section for a usual particle size distribution is most strongly affected by particles of size parameter 1 and larger.

Both particulate and molecular scattering are included in the profile of backscatter coefficient in Fig. 5. For a midlatitude standard atmosphere,

TABLE 6. Case study aerosol size distribution spectrum.

Height (km)	$\alpha(z)$	Log (excess concentration) 0.1 μm radius	1.5 μm radius
0.5	1.1	1.2	0.035
1	1.2	1.1	0.075
2	1.4	0.96	0.11
4	1.9	0.92	0.26

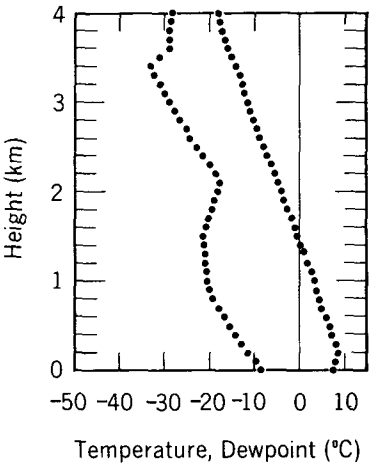

FIG. 6. Temperature and dew-point profiles taken at Denver on 8 March 1978. Sounding data from morning and evening are averaged.

the Rayleigh backscatter coefficient at 0.694 μm wavelength is 4.1×10^{-7} m^{-1} sr^{-1} at 0.4 km AGL and is 3.2×10^{-7} m^{-1} sr^{-1} at 2.8 km AGL. Thus, for the profile of 0.694 μm backscatter coefficient shown in Fig. 5, the molecular component is approximately 40% of the total backscatter at 0.4 km AGL and 90% of the total at 2.8 km AGL.

The ratio of visible to infrared backscatter coefficients increases generally with height, as expected from the more rapid falloff in concentration with height of the particles dominating infrared scattering compared to those dominant in visible backscatter. Table 5 gives visible-to-infrared backscatter ratios between 420 and 1140 over the height range 0.5–2 km for this particular case. The backscatter certainly does not scale as λ^{-4} (the Rayleigh small-scatterer approximation) nor does it have a constant scale at different heights. Incorporation of the size distribution slope into the wavelength scaling also does not provide a height-independent wavelength scaling power law. The data emphasize that visible-to-infrared backscatter ratios are dependent on the particular aerosol distribution (size spectrum and refractive index) present in the scattering volume.

d. Comparison of average backscatter and aerosol concentration profiles

We observe a correspondence in initial profile slopes between average backscatter and 1.5–3 μm radius particles. Calculations for 10.6 μm backscatter as a function of particle radius for a measured size distribution similar to ours (Post, 1978) peak at $r \approx 1.5$ μm.

The slopes of the backscatter and aerosol profiles are best compared graphically because the term β_c in Eq. (1) makes exponential coefficients m and p in Tables 2 and 3 not directly com-

parable. The initial falloff with height of the maximum backscatter model is more rapid than that for 0.5 μm radius particles, the same to within 4% of the falloff of the 1.5 μm particle profile, and less rapid than reductions in 0.1 and 3 μm particle concentrations with height. The average backscatter model decreases more rapidly with height than the maximum backscatter profile, approximately 12% faster than the 1.5 μm particle profile, and slower than the 3 μm profile. The minimum backscatter model exhibits the most rapid decrease with height of the quantities studied.

Above 2 km, the 10.6 μm backscatter profile falls off less rapidly than the 1.5 μm particle concentration profile and is more characteristic of the 0.5 μm profile. As the concentration of large particles relative to that of small particles decreases with height, the infrared backscatter becomes more dependent on the concentration of particles of radii < 1 μm. A comparison of profile slopes in Figs. 1 and 2 shows that in strong-scattering atmospheric conditions the infrared backscatter profile is characterized by the profile of smaller particles (near 0.5 μm radius) whereas for weak scattering the large-particle profile (particles > 3 μm radius) dominates at low altitudes. However, a wide range of particle sizes contributes to infrared backscatter.

The qualitative relationships between observed backscatter strength and most effective particle radius and the shift to smaller effective radius with height do not work well in the limit of small particle size. The falloff of the average 0.1 μm concentration up to 5.2 km is more rapid than that of 0.5 μm particle concentration, not less rapid. There is no strong indication in the data of an approach to a lower limit of particle density; no observed particle concentration profile shows the quasi-constant-with-height characteristic of the weak backscatter profile. Other effects must also be important. If the refractive index of the aerosols is not constant with height, then the backscatter cross section per particle changes.

Changes in relative humidity affect the real part of the visible-wavelength index of refraction of an aerosol particle (Hänel, 1976), and can also affect the particle size distribution by causing particle growth or shrinkage, depending on the previous history of the aerosol. The imaginary part of the index of refraction of liquid water is orders of magnitude larger at 10.6 μm than it is in the visible (Rusk *et al.*, 1971). Changes in humidity can have substantial effects on the infrared index of refraction of the particle. Thus, both the 0.694 and 10.6 μm aerosol backscatter can depend on relative humidity, as well as on aerosol concentration and size distribution spectra, and the humidity dependence of the backscatter may be different at different wavelengths.

e. Comparison with other work

We have not found other infrared backscatter profile measurements with which this work can be compared. However, many experiments on visible lidar backscatter, particularly in the stratosphere, have been reported (e.g., Grams and Fiocco, 1967; Fox *et al.*, 1973; McCormick *et al.*, 1978).

Surface values of the backscatter coefficient at 10.6 μm from other studies may be compared to the value from Fig. 1 of $\sim 1 \times 10^{-8}$ m^{-1} sr^{-1}. Rensch and Long (1970) gave calculations for 25 km visual range that lead to a 10.6 μm backscatter coefficient of 2.5×10^{-8} m^{-1} sr^{-1}. Visual ranges during our experiment averaged over 75 km, indicating significantly lower aerosol concentrations than used by Rensch and Long (1970). Hughes and Pike (1973) used a value of 1×10^{-8} m^{-1} sr^{-1} for typical 10.6 μm backscatter near the surface.

A total (angularly integrated) aerosol scattering coefficient σ of 5×10^{-11} cm^{-1} at 10.6 μm wavelength was observed by Muñoz *et al.* (1974) in a series of flights in the southwestern United States. This was an average of many flights over 300 m to 1500 m altitude. To estimate a differential backscatter cross section per unit volume (backscatter coefficient β) from the total scattering coefficient σ, one can use the mean of the four model aerosol results given by Shettle and Fenn[1] for 10.59 μm wavelength. This value is $\beta/\sigma \approx 0.025$ sr^{-1} $\pm$ 3 dB, where the uncertainty covers the range of (spherical particle) model results. The use of this conversion factor allows an estimate of $\beta = 1.2 \times 10^{-10}$ m^{-1} sr^{-1} $\pm$ 3 dB to be made from the extinction values reported by Muñoz *et al.* Our model of the average scattering profile (based on the measurements) gives $\beta = 1.5 \times 10^{-9}$ m^{-1} sr^{-1} $\pm$ 2.5 dB at 1500 m, and a minimum modeled scatter of $\beta = 3.9 \times 10^{-11}$ m^{-1} sr^{-1} $\pm$ 2.5 dB at that altitude. The fact the average of Muñoz *et al.* is less than our average is not surprising because the earlier study reported visibilities > 150 km in many cases. Muñoz *et al.* also observed the large spatial variability in backscatter coefficient that we observed on individual data runs.

Although no previous direct measurements of backscatter coefficient profiles at 10.6 μm have been made, Post (1979) presented model profiles for aerosol backscatter at 10.6 μm based on observations of visible wavelength backscatter, assumed aerosol properties and Mie calculations. The calculated models are sensitive to the index of refrac-

[1] Shettle, E. P., and R. W. Fenn, 1976: Models of the atmosphere aerosols and their optical properties. *NATO, AGARD Conference Proceedings*, No. 183, *Optical Propagation in the Atmosphere*, AGARD-CP-183 [NTIS ADA 028-615]. 2-1–2-16.

tion of the particles, which was assumed to be a compromise value between water and minerals, and to particle shape, which was assumed spherical. The minimum backscatter coefficient profile modeled by Post is at least four times larger than the average of our measurements for the same height above the surface. The minimum value of the Post model at the surface is also approximately four times larger than previous surface measurements (Rensch and Long, 1970; Hughes and Pike, 1973) and at 1.5 km above the surface is more than 10 times larger than the measurements of Muñoz *et al.* (1974).

Duntley *et al.* (1977)[2] performed airborne measurements of total volume scattering coefficient (not backscatter) in the visible. These workers observed total scattering coefficients in the range 1×10^{-5} m^{-1} to 1×10^{-3} m^{-1} in the first 6 km of the atmosphere. Using the typical value of backscatter to total scatter coefficient at visible wavelengths of $\beta/\sigma \approx 0.04 \pm 0.03$ sr^{-1}, which comes from work summarized by Collis and Russell (1976), yields a range of 1×10^{-7} to 1×10^{-4} m^{-1} sr^{-1} for the visible backscatter coefficient in the 0–6 km altitude region. Our results at 0.694 μm fall within the lower end of this rather broad range. Aerosol data are not given for the total volume scattering work. In most cases Duntley *et al.* (1977)[2] found the scattering coefficient decreasing with wavelength, which we observe in our data taken over a wider wavelength span.

We found in the case study results that backscatter did not track the relative humidity profile in either the infrared or red lidar profiles. This behavior was also noted by Duntley *et al.* (1977).[2] Rubio (1977)[3] observed a lack of correlation between relative humidity and ruby lidar backscatter, although in his experiment the backscatter changed abruptly whereas the temperature and humidity profiles did not.

The slopes of our aerosol size distribution function [coefficient $\alpha(z)$ in Tables 4 and 6] for radii > 1 μm at lower altitudes are less than the averages for dry aerosols found by DeLuisi *et al.* (1972). However, our bimodal size spectra are not directly comparable to a simple power-law distribution. The effect of the large excess concentration at 0.1 μm radius is to yield an effective $\alpha(z)$ for our data much larger than that shown in Tables 4 and 6, where the small-particle peak is separated out. Post (1978), using a different *in situ* particle sizing technique, also found a smaller $\alpha(z)$ than generally observed. At 4 km above the surface, our observed $\alpha(z)$ approaches the more commonly observed value of ~3. Condensation growth for *in situ* aerosols (in contrast to dried aerosol samples) in the 1–3 μm range may partially account for the difference in $\alpha(z)$ values. Our overall particle concentrations are found to be within the ranges of the models of DeLuisi *et al.*

4. Comments

In the cases studied, the infrared (10.6 μm) backscatter coefficient in the first 5 km of the atmospheric boundary layer ranged between ~0.4 $\times 10^{-11}$ m^{-1} sr^{-1} and 2×10^{-8} m^{-1} sr^{-1}. The reduction in backscatter was found to be as large as 100 times between 200 m altitude and 2 km in the case of weak scattering.

Because the infrared backscatter depends on more variables than aerosol concentration and size distribution, we suggest that future studies include *in situ* data on aerosol refractive index at 10.6 μm. Additional aerosol and backscatter profiles would help quantify the statistics of time and space variation of infrared backscatter.

Acknowledgments. These data could not have been obtained without the ruby lidar measurement expertise of N. L. Abshire and the help of H. L. Ericson with the airborne aerosol measurements. D. L. Wellman was in charge of the aerosol instrumentation. M. J. Post assisted in the performance and analysis of the calibration. We appreciate the interest of C. G. Little in the backscatter profile measurements. This study was supported in part by the U.S. Environmental Protection Agency under agreement EPA-IAG-D5-0693, 79 BEB.

[2] Duntley, S. Q., R. W. Johnson and J. I. Gordon, 1977: Airborne measurements of atmospheric volume scattering coefficients in northern Europe, spring 1976. Air Force Geophys. Lab. Rep. AFGL-TR-77-0078, 151 pp. [See also: Airborne measurements of optical atmospheric properties, summary and review III. Air Force Geophys. Lab. Rep. AFGL-TR-78-0286, 117 pp.]

[3] Rubio, R., 1977: Investigation of abrupt decreases in atmospherically backscattered laser energy. U.S. Army Electronics Command Rep. ECOM-5835, 22 pp.

REFERENCES

Collis, R. T. H., and P. B. Russell, 1976: Lidar measurement of particles and gases by elastic backscattering and differential absorption. *Laser Monitoring of the Atmosphere: Topics in Applied Physics,* Vol. 14, E. D. Hinkley, Ed., Springer-Verlag, 71–151.

DeLuisi, J. J., I. H. Blifford, Jr., and J. A. Takamine, 1972: Models of tropospheric aerosol size distribution derived from measurements at three locations. *J. Geophys. Res.*, **77**, 4529–4538.

Dickson, L. D., 1970: Characteristics of a propagating Gaussian beam. *Appl. Opt.*, **9**, 1854–1861.

Fiocco, G., G. Benedetti-Michelangeli, K. Maischberger and E. Madonna, 1971: Measurement of temperature and aerosol to molecule ratio in the troposphere by optical radar. *Nature, Phys. Sci.* **229**, 78–79.

Fox, R. J., G. W. Grams, B. G. Schuster and J. A. Weinman, 1973: Measurements of stratospheric aerosols by airborne laser radar. *J. Geophys. Res.*, **78,** 7789–7801.

Grams, G., and G. Fiocco, 1967: Stratospheric aerosol layer during 1964 and 1965. *J. Geophys. Res.*, **72,** 3523–3542.

Hänel, G., 1976: The properties of atmospheric aerosol particles as functions of the relative humidity at thermodynamic equilibrium with the surrounding moist air. *Advances in Geophysics*, Vol. 19, H. E. Landsberg and J. Van Mieghem, Eds., Academic Press, 73–188.

Hughes, A. J., and E. R. Pike, 1973: Remote measurement of wind speed by laser Doppler systems. *Appl. Opt.*, **12,** 597–601.

Lundgren, D. A., F. S. Harris, Jr., W. H. Marlow, M. Lippmann, W. E. Clark and M. D. Durham, Eds., 1979: *Aerosol Measurement*, Gainesville, University Presses of Florida, 716 pp.

McCormick, M. P., T. J. Swissler, W. P. Chu and W. H. Fuller, Jr., 1978: Post-volcanic stratospheric aerosol decay as measured by lidar. *J. Atmos. Sci.*, **35,** 1296–1303.

Muñoz, R. M., H. W. Mocker and L. Koehler, 1974: Airborne laser Doppler velocimeter. *Appl. Opt.*, **13,** 2890–2898.

Post, M. J., 1978: Experimental measurements of atmospheric aerosol inhomogeneities. *Opt. Lett.*, **2,** 166–168.

——, 1979: Effects of the earth's atmosphere on a spaceborne IR Doppler wind-sensing system. *Appl. Opt.*, **18,** 2645–2653.

Rensch, D. B., and R. K. Long, 1970: Comparative studies of extinction and backscattering by aerosols, fog, and rain at 10.6 μ and 0.63 μ. *Appl. Opt.*, **9,** 1563–1573.

Rusk, A. N., D. Williams and M. R. Query, 1971: Optical constants of water in the infrared. *J. Opt. Soc. Amer.*, **61,** 895–903.

Schwiesow, R. L., and R. E. Cupp, 1980: Calibration of a CW infrared Doppler lidar. *Appl. Opt.*, **19,** 3168–3172.